ISSN 0023-1584, Kinetics and Catalysis, 2008, Vol. 49, No. 4, pp. 581–586. © MAIK "Nauka/Interperiodica" (Russia), 2008.
Original Russian Text © Yu.V. Larichev, S.E. Malykhin, 2008, published in Kinetika i Kataliz, 2008, Vol. 49, No. 4, pp. 607–612.

III INTERNATIONAL CONFERENCE "CATALYSIS: FUNDAMENTALS AND APPLICATIONS"

New Opportunities for the Identification of Oxide Clusters in Supported Ru/MgO Catalysts

Yu. V. Larichev and S. E. Malykhin

Boreskov Institute of Catalysis, Siberian Branch, Russian Academy of Sciences, Novosibirsk, 630090 Russia
e-mail: larichev@catalysis.ru

Received June 11, 2007

Abstract—The Ru/MgO systems were studied using XPS, transmission electron microscopy, and X-ray diffraction analysis. It was found that from 25 to 75% of the supported metal can occur in an X-ray amorphous form with a particle size of smaller than 3 nm. The insertion of supported metal ions into the support structure was absent. A comparison between the valence band XPS spectra and the corresponding densities of states calculated by quantum-chemical methods indicated that the X-ray amorphous portion of the metal can occur as both metal and oxide clusters depending on the precursor of ruthenium.

DOI: 10.1134/S0023158408040198

INTRODUCTION

Various valence states of a supported metal catalyst (metal, oxide, inserted ions, etc.) exhibit different activities and selectivities in catalytic processes. As a rule, after a reduction treatment, the supported noble metal particles are metal nanoparticles with characteristic sizes from 1 to 50 nm (depending on the types of the metal and the support and on catalyst preparation conditions) [1]. New states of a supported metal can be observed with decreasing particle size. For example, metal ions can be inserted into the support to form various structures [2]; supported metal oxide species can be stabilized on the support [3]. Depending on the valence state of a supported metal, metal particles behave as active sites for a main or side reaction and, correspondingly, affect the yield of the target product. The concentration of active sites can decrease to cause a surcharge of a noble metal in the course of catalyst preparation. Thus, the supported metal species should be fully identified in supported metal catalysts. This is of particular importance for small particles of size less than 1.5 nm. In transmission electron microscopy (TEM), which is a widely used technique, an almost atomic resolution can be achieved in special experiments [4]; however, objects of size smaller than 1 nm cannot be recognized in the case of supported catalysts because of the low contrast of the image. Because of this, as a rule, the valence state of a metal in these particles cannot be determined.

The aim of this work was to identify the valence states of ruthenium supported on magnesium oxide in particles with sizes smaller than 2 nm using XPS. This system (Ru/MgO), which is a convenient model system, was studied previously [5]. The results obtained in the study of the above system can be applied to commercial supported catalysts.

EXPERIMENTAL

Sample Preparation

Three samples of supported Ru/MgO catalysts, ruthenium black, and ruthenium oxide (RuO_2) were chosen for this study. Two types of MgO were used as supports: a commercial reagent (MgO–R) and MgO prepared at the Boreskov Institute of Catalysis (Novosibirsk) with different surface areas, which were determined by the BET method from the low-temperature adsorption of N_2 (Table 1).

The active component precursor $Ru(OH)Cl_3$ or $Ru(acac)_3$ was supported by incipient wetness impregnation from an acetone solution. The catalyst sample was reduced in a flow of hydrogen in a glass tube reactor at $T = 450$°C for 6 h. After the reduction, the sample was cooled in a flow of H_2 to room temperature, removed from the reactor, and kept under argon. The sample preparation procedure was considered in more detail elsewhere [5]. Table 2 summarizes the weight concentrations of ruthenium in the prepared samples.

Ruthenium black was prepared by the reduction of $RuOHCl_3$ with formalin in an aqueous alkali solution on heating to 80°C [6]. After washing and drying, the black powder was additionally reduced in a flow of hydrogen on heating to 350°C. Ruthenium oxide was prepared by the calcination of ruthenium hydroxide at

Table 1. Specific surface areas and pore characteristics of parent supports

Support	S_{sp}, m^2/g	V, cm^3/g	R_{pore}, nm
MgO–R	22	0.09	20.0
MgO	200	0.42	9.0

Table 2. Ruthenium contents of the samples

Sample	Ru content, wt %
Ru(Cl)/MgO*	5.0
Ru(Cl)/MgO–R*	4.4
Ru(AA)/MgO**	5.0

*Prepared from $Ru(OH)Cl_3$.
**Prepared from $Ru(acac)_3$.

Table 3. Ru $3d_{5/2}$ binding energies and line widths at half heights for ruthenium samples

Sample	E_b, eV	Width at half height, eV
Ru(Cl)/MgO	280.5	3.0
Ru(Cl)/MgO–R	280.4	2.3
Ru(AA)/MgO	280.6	3.6
Ru (black)	280.2	1.3
RuO_2	281.4	2.7
$Ru(OH)Cl_3$	282.0	2.3

T = 150°C; in turn, ruthenium hydroxide was prepared from $Ru(OH)Cl_3$ by precipitation with NaOH. According to X-ray diffraction (XRD) data, the resulting compound corresponded to the structure of RuO_2.

Sample Characterization

The resulting supported samples were analyzed by high-resolution electron microscopy to obtain information on their morphology and microstructure. In these studies, a JEM 2010 transmission electron microscope with a line resolution of 0.14 nm and an accelerating voltage of 200 kV was used. Additionally, XRD analysis was used to obtain information on the phase composition and the sizes of coherent scattering regions (CSRs). The measurements were performed on an HZG-4 diffractometer. The adsorption characteristics of the supports, such as specific surface areas, pore volumes, and average pore sizes, were obtained using an ASAP-2400 system. The electronic properties of the samples were studied using XPS. The spectra were recorded on a VG ESCALAB HP electron spectrometer with the use of unmonochromated AlK_α radiation ($h\nu$ = 1486.6 eV; 200 W). The binding energy (E_b) scale of the spectrometer was precalibrated using the peak positions of the Au $4f_{7/2}$ (84.0 eV) and Cu $2p_{3/2}$ (932.6 eV) core levels. An internal standard technique was used for calibrating photoelectron lines, in particular, for eliminating the charging effect, which occurs in an XPS study of nonconducting samples. In this case, the Mg 2s line with E_b = 88.1 eV from the MgO support was used as a reference; it is believed that this line remained unchanged in the course of experiments. The charging value was determined as the difference between the measured binding energy and the tabulated value of E_b. The positions of photoelectron lines from the other elements were shifted by this value. Before measuring the spectra, the samples of supported systems were pressed into Ni gauze and placed in the preparation chamber of the spectrometer (the residence time of the samples in air during this procedure was no longer than 5 min). In the spectrometer, the samples were additionally treated with hydrogen under batch conditions at 350°C and a pressure of 0.1 MPa for 1 h.

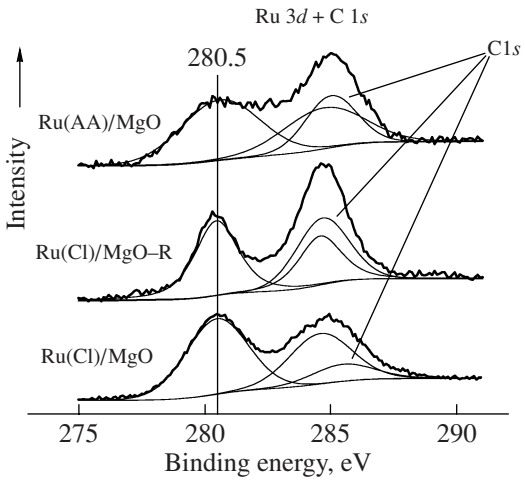

Fig. 1. Ru 3d XPS spectra of the test samples. Arrows indicate the C 1s peaks overlapping with the Ru $3d_{3/2}$ peaks.

Quantum-Chemical Calculations

The curves of the densities of states were calculated based on the density functional theory (local density approximation (LDA); PW91 functional [7]) using the all-electron full-potential linearized augmented-plane wave (FP LAPW) method. The EXCITING software package [8] was used for the calculations. A ruthenium metal crystal and a ruthenium oxide (RuO_2) crystal were used as models for the calculations. The unit cell parameters found from the experimental structural data are $P6_3/mmc$, a = 0.2758 nm, and c = 0.42819 nm (JCPDS 06-0663) for Ru and $P4_2/mnm$, a = 0.449946 nm, and b = 0.310714 nm (JCPDS 40-1290) for RuO_2. The integration of the Brillouin zone was performed using a 16 × 16 × 16 k-point sampling for ruthenium metal and a 4 × 4 × 4 point sampling for ruthenium oxide. The densities of states were calculated over a range of ±13.6 eV with respect to the Fermi energy.

RESULTS AND DISCUSSION

Figure 1 shows the Ru 3d spectra of ruthenium samples. After considering the effects of final states (differential charging effect), the Ru $3d_{5/2}$ binding energies in

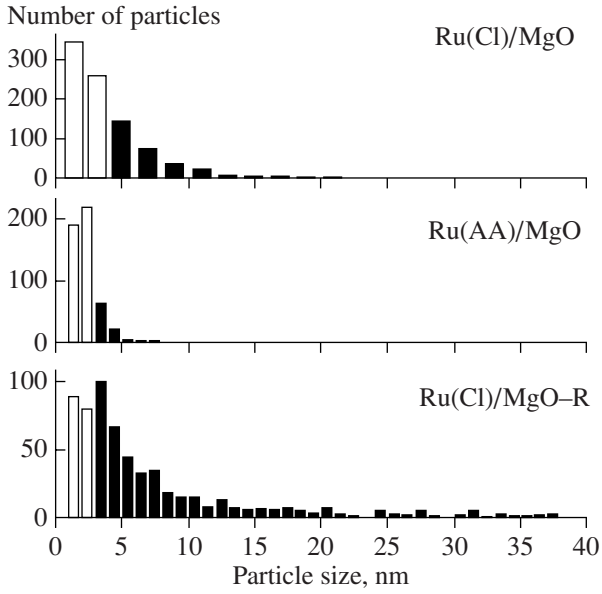

Fig. 2. Particle size distribution in the tested samples. The numbers of particles with sizes smaller than 3 nm are shown in white.

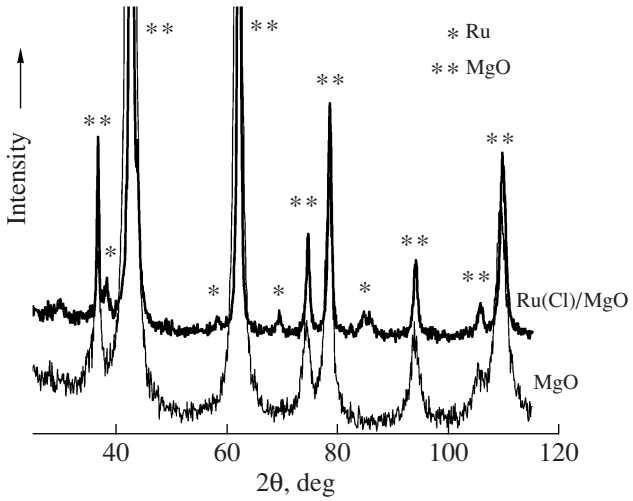

Fig. 3. X-ray diffraction patterns of MgO and Ru(Cl)/MgO.

Ru/MgO samples were ~280.5 eV (Table 3) [5, 9, 10]. The Ru $3d_{5/2}$ binding energy in bulk ruthenium metal (as Ru black) was somewhat lower (280.2 eV), which is consistent with tabulated data [11]. The Ru $3d_{5/2}$ binding energies in Ru(III) and Ru(IV) compounds were much greater than that of Ru^0.

As can be seen in Fig. 1, the spectra are broad (peak width at half height of ~3 eV). This phenomenon can be observed because of both sample charging after photoemission and the occurrence of additional states. Because the spectra are sufficiently symmetrical and they are adequately described using a single state, a reliable conclusion on the occurrence of additional states of ruthenium in the samples cannot be drawn from these data.

According to TEM data, supported ruthenium occurred in the samples as round-shaped metal particles. Ruthenium oxides were not detected. Bar diagrams (Fig. 2) were plotted based on micrographs, and average linear ($\langle d_l \rangle$) and volumetric surface ($\langle d_{vs} \rangle$[1]) ruthenium particle sizes were determined from these diagrams (Table 4). As can be seen in the bar diagrams, the numbers of small particles (white) strongly varied depending on samples. The diffraction patterns exhibited reflections due to the support and ruthenium metal (Fig. 3). Reflections due to ruthenium oxide were not observed. The CSR value for ruthenium particles was approximately consistent with the weight-average particle size determined from TEM data.

[1] $\langle d_l \rangle = \Sigma d_i/N$; $\langle d_{vs} \rangle = \Sigma_i d_i^3 / \Sigma_i d_i^2$, where N is the total number of particles measured in electron micrographs and i is the summation index.

Note that the unit cell parameter of the MgO support decreased from 0.4224 to 0.4212 nm after supporting and reducing ruthenium. It would be expected that the unit cell parameter would decrease because of cell compression upon the insertion of ruthenium ions into the support lattice. However, it is our opinion that the decrease in the unit cell parameter was due to a decrease in the concentration of hydroxyl groups in the support upon calcination. Thus, the unit cell parameter of the MgO–R support precalcined at 800–900°C was much smaller than that of MgO (0.4213 against 0.4224 nm); however, the unit cell parameter of MgO–R in Ru(Cl)/MgO–R remained almost unchanged. Thus, the compression of the support lattice was due to the properties of the support rather than the insertion of ruthenium ions into the support.

The unit cell parameters of supported ruthenium are consistent with the unit cell parameters found for ruthenium black (a = 0.270(4) nm and c = 0.428(2) nm for supported ruthenium or a = 0.2707(2) nm and c = 0.4280(3) nm for bulk ruthenium) within the limits of experimental error in XRD analysis.

To determine whether ruthenium completely constituted a Ru phase with the measured CSR values, we performed calibration with the mechanical mixtures of

Table 4. Particle sizes (nm) of the tested samples determined by TEM and XRD analysis

Sample	$\langle d_l \rangle$	$\langle d_{vs} \rangle$	CSR
Ru(Cl)/MgO–R	7.2	27	30
Ru(Cl)/MgO	3.5	8.5	10
Ru(AA)/MgO	2.2	3.3	6.0
Ru (black)	33	65	45
RuO_2	–	–	13

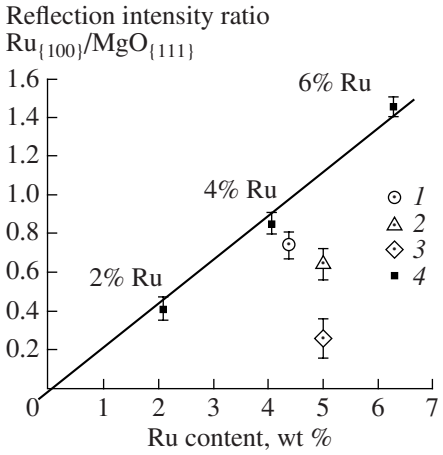

Fig. 4. Fractions of X-ray amorphous ruthenium in the (*1*) Ru(Cl)/MgO–R, (*2*) Ru(Cl)/MgO, and (*3*) Ru(AA)/MgO samples and (*4*) calibration mixtures of MgO and Ru black as the dependence of the intensity ratio between the (100) and (111) reflections of the Ru and MgO phases, respectively, on the total ruthenium content.

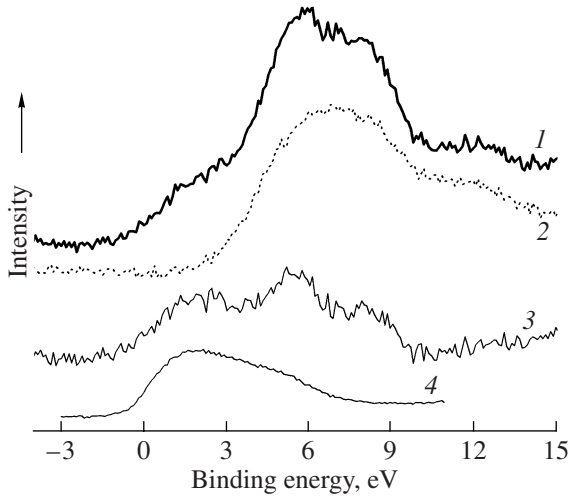

Fig. 5. Valence band spectra of (*1*) Ru(Cl)/MgO and (*2*) MgO, (*3*) the difference spectrum, and (*4*) the valence band spectrum of bulk ruthenium.

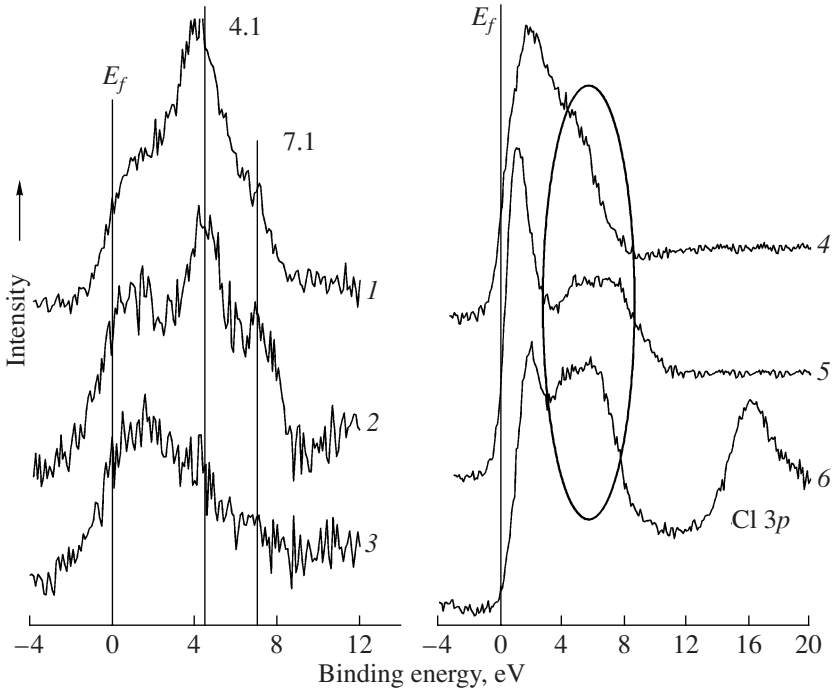

Fig. 6. Difference valence band spectra of the (*1*) Ru(Cl)/MgO–R, (*2*) Ru(Cl)/MgO, and (*3*) Ru(AA)/MgO supported systems and the valence band spectra of reference samples: (*4*) Ru black, (*5*) RuO_2, and (*6*) $Ru(OH)Cl_3$. The region corresponding to the Ru 4*d*5*s* and O 2*p* bands is marked with an oval.

Ru black and MgO containing 2, 4, and 6% ruthenium (Fig. 4). We measured the ratio between the integrated intensities of the (100) and (111) reflections of the Ru and MgO phases, respectively, depending on the ruthenium concentration. The resulting dependence for the Ru(Cl)/MgO sample demonstrated that diffraction was observed in 40% supported metal, whereas the remaining 60% occurred in an X-ray amorphous state. In the Ru(Cl)/MgO–R sample, diffraction was observed in 76% supported metal; the remaining 24% occurred in an X-ray amorphous state. On the contrary, in the Ru(AA)/MgO sample, the major portion of the supported metal (75%) was in X-ray amorphous form. The portion of ruthenium that did not manifest itself as diffraction peaks can occur in an ultrafine state (≤2 nm) or as an ultrafine oxide. It is likely that the presence of this

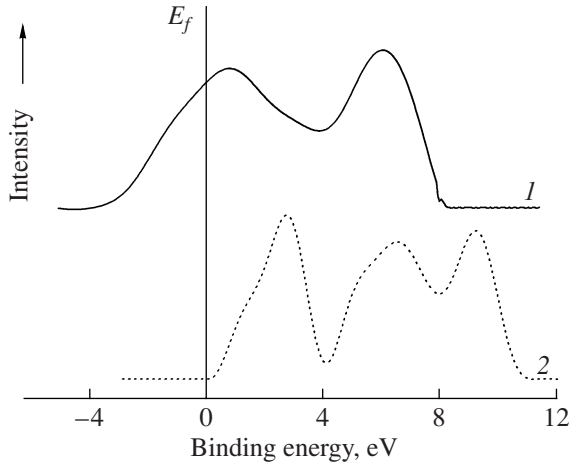

Fig. 7. Calculated densities of states for the structures of (*1*) Ru and (*2*) RuO_2.

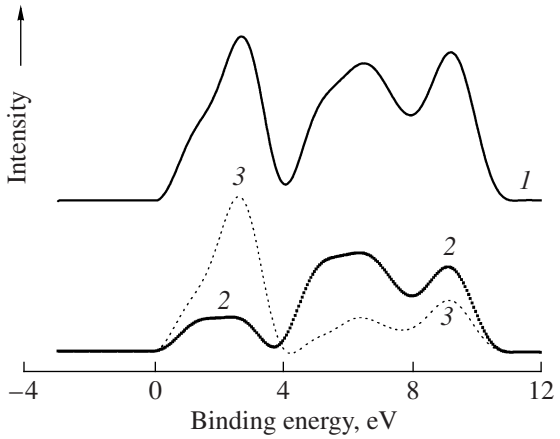

Fig. 8. (*1*) Calculated density of states for the structure of RuO_2 and partial densities of states for (*2*) O and (*3*) Ru.

portion of the metal as ions incorporated into the support lattice can be excluded.

Figure 5 shows the difference valence band XPS spectra of supported samples and the spectrum of bulk ruthenium for comparison. The difference spectra were obtained by subtracting the corresponding spectrum of parent MgO from the valence band spectra of Ru/MgO. In the difference spectra (Fig. 6), two bands with different intensities at 4.1 and 7.1 eV are present in addition to a broad band due to ruthenium metal. Note that these bands are absent from the difference spectrum of the Ru(AA)/MgO sample. As can be seen in Fig. 6, the difference spectra of the Ru(Cl)/MgO and Ru(Cl)/MgO–R samples are qualitatively similar to the valence band spectra of $Ru(OH)Cl_3$ and RuO_2.

According to quantum-chemical calculations (Fig. 7), a good agreement is generally observed between the calculated densities of states and the experimental valence band spectra of Ru and RuO_2. Figure 8 shows the partial densities of states for O and Ru atoms in the structure of RuO_2. It can be seen that the range from 0 to 4 eV primarily accomodates the Ru 4*d*5*s* valence band, whereas the range from 4 to 10 eV primarily accomodates the O 2*p* valence band. Our assignment is consistent with data published by Sven et al. [12], who studied the oxidation of bulk ruthenium.

Thus, additional peaks at 4.1 and 7.1 eV in the difference spectra can be assigned to RuO_2 nanoparticles, which have a band structure and sizes from 0.6–0.7 nm (about 70 atoms) to 1.0–1.5 nm (about 300–900 atoms). At smaller sizes (<0.6 nm), an oxide nanoparticle does not have a broad band structure, but it has only a set of narrow lines, which cannot be identified because of the low resolution of the XPS spectrometer. At greater sizes (≥2 nm), an oxide nanoparticle can be identified using TEM. The only stable ruthenium oxide is volatile RuO_4. Based on these data, we can assume the occurrence of large clusters and/or nanoparticles of RuO_2 in the Ru(Cl)/MgO and Ru(Cl)/MgO–R samples. The occurrence of ultrafine RuO_2 in Ru(Cl)/MgO and Ru(Cl)/MgO–R and the absence of ultrafine RuO_2 from Ru(AA)/MgO can be explained assuming that the $Ru(OH)Cl_3$ compound on the surface of MgO is partially hydrolyzed with the formation of $Ru(OH)_4$ in the presence of trace water in acetone followed by decomposition to RuO_2. The $Ru(acac)_3$ compound is stable under the given conditions, and it does not undergo decomposition of this kind. The stability of RuO_2 upon the reduction of the sample in hydrogen can be explained by the occurrence of epitaxial interactions between RuO_2 and MgO layers. According to Gao et al. [13], this epitaxial interaction really occurs in the RuO_2/MgO system between the {110} and {100} layers of RuO_2 and MgO, respectively. Thus, epitaxy between RuO_2 and MgO stabilizes RuO_2 oxide nanoparticles upon the treatment of the sample in hydrogen at 450°C.

CONCLUSIONS

We demonstrated that valence band spectra can be used in the identification of nanoparticles and clusters. We found that RuO_2 oxide nanoparticles occur in the Ru(Cl)/MgO and Ru(Cl)/MgO–R catalysts in addition to Ru metal nanoparticles. Oxide nanoparticles of this type were not detected in Ru(AA)/MgO.

ACKNOWLEDGMENTS

We are grateful to B.L. Moroz, E.M. Moroz, and V.I. Zaikovskii for their assistance.

REFERENCES

1. Schloegl, R., in *Handbook of Heterogeneous Catalysis*, Ertl, G., Knoezinger, H., and Weitkamp, J., Eds., Weinheim: Wiley–VCH, 1997, vol. 4, p. 1697.

2. Bera, P., Gayen, A., Hegde, M.S., Lalla, N.P., Spadaro, L., Frusteri, F., and Arena, F., *J. Phys. Chem. B*, 2003, vol. 107, p. 6122.
3. Silva, J.W. and Cobo, A.J.G., *Appl. Catal., A*, 2003, vol. 252, p. 9.
4. O'Keefe, M.A., Allard, L.F., Pennycook, S.J., and Blom, D.A., *Microsc. Microanal.*, 2006, vol. 12, p. 162.
5. Larichev, Yu.V., Moroz, B.L., Moroz, E.M., Zaikovskii, V.I., Yunusov, S.M., Kalyuzhnaya, E.S., Shur, V.B., and Bukhtiyarov, V.I., *Kinet. Katal.*, 2005, vol. 46, no. 6, p. 940 [*Kinet. Catal.* (Engl. Transl.), vol. 46, no. 6, p. 891].
6. Kobayashi, M. and Shirasaki, T., *J. Catal.*, 1973, vol. 28, p. 289.
7. Wang, P. and Alder, C., *Phys. Rev. B: Condens. Matter*, 1992, vol. 45, p. 13 244.
8. Dewhurst, J.K., Sharma, S., Ambrosch-Draxl, C., et al., *The EXCITING FP-LAPW Code*, Graz, Austria, 2004; http://exciting.sourceforge.net/.
9. Larichev, Y.V., Moroz, B.L., Prosvirin, I.P., Bukhtiyarov, V.I., and Likholobov, V.A., *Chem. Sustainable Dev.*, 2003, vol. 11, p. 155.
10. Bukhtiyarov, V.I., Prosvirin, I.P., and Kvon, R.I., *J. Electron Spectrosc. Relat. Phenom.*, 1996, vol. 77, p. 7.
11. *Practical Surface Analysis*, Briggs, D. and Seah, M.P., Eds., Chichester: Wiley, 1990, vol. 1.
12. Sven, J.Y., Adnot, A., and Kaliaguine, S., *Appl. Surf. Sci.*, 1991, vol. 51, p. 47.
13. Gao, Y., Bai, G., Liang, Y., et al., *J. Mater. Res.*, 1997, vol. 12, no. 7, p. 1844.